Pure appl. geophys. 164 (2007) 217–244
0033–4553/07/010217–28
DOI 10.1007/s00024-006-0152-9

Pure and Applied Geophysics

A Godunov-Type Scheme for Atmospheric Flows on Unstructured Grids: Euler and Navier-Stokes Equations

Nash'at Ahmad,[1] Zafer Boybeyi,[2] Rainald Löhner,[2] and Ananthakrishna Sarma[1]

Abstract—In recent years there has been a growing interest in using Godunov-type methods for atmospheric flow problems. Godunov's unique approach to numerical modeling of fluid flow is characterized by introducing physical reasoning in the development of the numerical scheme (van Leer, 1999). The construction of the scheme itself is based upon the physical phenomenon described by the equation sets. These finite volume discretizations are conservative and have the ability to resolve regions of steep gradients accurately, thus avoiding dispersion errors in the solution. Positivity of scalars (an important factor when considering the transport of microphysical quantities) is also guaranteed by applying the *total variation diminishing* condition appropriately. This paper describes the implementation of a Godunov-type finite volume scheme based on unstructured adaptive grids for simulating flows on the meso-, micro- and urban-scales. The Harten-Lax-van Leer-Contact (HLLC) approximate Riemann solver used to calculate the Godunov fluxes is described in detail. The higher-order spatial accuracy is achieved via gradient reconstruction techniques after van Leer and the *total variation diminishing* condition is enforced with the aid of slope-limiters. A multi-stage explicit Runge-Kutta time marching scheme is used for maintaining higher-order accuracy in time. The scheme is conservative and exhibits minimal numerical dispersion and diffusion. The subgrid scale diffusion in the model is parameterized *via* the Smagorinsky-Lilly turbulence closure. The scheme uses a non-staggered mesh arrangement of variables (all quantities are cell-centered) and requires no explicit filtering for stability. A comparison with exact solutions shows that the scheme can resolve the different types of wave structures admitted by the atmospheric flow equation set. A qualitative evaluation for an idealized test case of convection in a neutral atmosphere is also presented. The scheme was able to simulate the onset of Kelvin-Helmholtz type instability and shows promise in simulating atmospheric flows characterized by sharp gradients without using explicit filtering for numerical stability.

Key words: Atmospheric flows, Godunov method, unstructured grids, Riemann solver.

1. Introduction

Traditionally, finite-difference discretizations of centered schemes such as the Leapfrog scheme have been favored for discretizing the atmospheric flow equation set. These types of schemes have large amounts of dispersion errors (non-physical

[1] Center for Atmospheric Physics, Science Applications International Corporation, McLean, VA 22102, U.S.A. E-mail: ahmadn@saic.com
[2] School of Computational Sciences, George Mason University, Fairfax, VA 20030, U.S.A.

spurious oscillations), which can contaminate the numerical results (CARPENTER *et al.*, 1990). At smaller spatial and temporal scales (non-hydrostatic meso-scale flows), large gradients of velocities and other physical quantities can develop and the local accuracy becomes important. The application of the Leapfrog scheme on smaller scales requires explicit time filtering for stability. The Asselin time filter, which is often used, degrades the accuracy of the scheme in time (DURRAN, 1991; MENDEZ-NÚÑEZ and CARROLL, 1993). Furthermore, the scheme can introduce false negatives in important scalar microphysical quantities. To avoid false negatives, either positive definite schemes (SMOLARKIEWICZ, 1984; BOTT, 1989) or Flux Corrected Transport (FCT)-type schemes (BORIS and BOOK, 1973; ZALESAK, 1979) are sometimes used to advect scalar quantities.

A number of studies have been conducted on the design and implementation of upwind schemes (SMOLARKIEWICZ, 1984; TREMBACK *et al.*, 1987; BACON *et al.*, 2000; AHMAD *et al.*, 2006). The use of upwind schemes in operational models however has been limited. The upwind scheme is only first-order accurate and therefore highly diffusive and its higher-order extensions can be computationally expensive compared to, e.g., the Leapfrog scheme. In the past decades, there has been an immense increase in both CPU speed and available memory and these advances in computer hardware are projected to continue. It is therefore not only feasible but also essential to explore the use of better numerical schemes including higher-order upwind schemes for atmospheric modeling. In this study high-resolution Godunov-type methods are explored for solving the nonlinear equations arising in atmospheric flows. These finite volume discretizations are conservative and have the ability to resolve regions of steep gradients accurately, thus avoiding dispersion errors in the solution.

Over the past two decades, Godunov-type methods (GODUNOV, 1959) have gained wide popularity in the scientific computing community for solving the systems of hyperbolic conservation laws. Godunov's unique approach to numerical modeling of fluid flow is characterized by introducing physical reasoning in the development of the numerical scheme (VAN LEER, 1999). The construction of the scheme itself is based upon the physical phenomenon described by the equation sets. The scheme and its higher-order extensions have been used mostly for aerospace-related simulations (LUO *et al.*, 2003). CARPENTER *et al.* (1990) have applied the method for atmospheric flows using an exact Riemann solver in conjunction with the Piecewise Parabolic Method (COLLELA and WOODWARD 1984). CARPENTER *et al.* show the inherent strengths of Godunov-type methods by providing a comparison with the Multidimensional Positive Definite Advection Transport Algorithm (SMOLARKIEWICZ, 1984) and the Leapfrog schemes. The important role Godunov-type methods can play in accurately resolving atmospheric phenomena characterized by steep gradients is also pointed out.

Fronts, for example, are typically associated with large horizontal temperature and wind gradients and vertical wind shear. Strong convection in supercell

thunderstorms can produce tornadoes, large hail, strong winds (in excess of 50 ms^{-1}), lightning and flash floods (BROOKS and DOSWELL, 1993). Drylines are characterized by a strong moisture gradient in the planetary boundary layer. In the Great Plains this gradient can be up to several degrees Celsius, which is considerably larger than the climatological average of 0.04°C km^{-1} in the dewpoint temperature (SHAW *et al.*, 1997). Drylines can trigger strong convective activity and winds in excess of 50 miles per hour have been observed. In tornadoes (F5 category), winds between 125 and 140 ms^{-1} have been observed. Hurricanes are yet another example of an atmospheric process which is characterized by extreme gradients of velocities and potential temperature (EMANUEL, 1988; GOPALAKRISHNAN *et al.*, 2002).

Different authors have explored the possible use of alternative finite volume schemes for atmospheric modeling (e.g., BOTTA *et al.*, 2004; HUBBARD and NIKIFORAKIS, 2003; LIN *et al.*, 1994; MÜLLER, 1992). The application for atmospheric modeling, however, has been limited mostly to solving the scalar transport equation. In this study a high-resolution Godunov-type scheme for the Euler equations governing atmospheric flows is developed and then extended to the Navier-Stokes equations. This work differs from CARPENTER *et al.*'s (1990) work in the following aspects:

- The equations and the solution methodology are in the Eulerian frame of reference rather than Lagrangian.
- An approximate Riemann solver is employed instead of an exact solver to calculate the Godunov fluxes. The computational cost of an exact Riemann solver can become prohibitive for simulations in three dimensions. The solution obtained by an approximate Riemann solver is comparable to the solution from an exact solver — the computational overhead, however is greatly reduced.
- The scheme is extended to the Navier-Stokes equations (the subgrid scale diffusion is treated as a source term).
- The solver is implemented on unstructured meshes.

In recent years there has been a growing interest in the use of unstructured adaptive grids for modeling atmospheric transport and diffusion problems (BACON *et al.*, 2000; BOYBEYI *et al.*, 2001; SMOLARKIEWICZ and SZMELTER, 2005). The unstructured grids provide the ability to discretize complex computational domains with relative ease. The capability to resolve the inherently multi-scale nature of atmospheric flows in a computationally efficient manner (*via* static or dynamic grid adaptation) can also be achieved. The unstructured grids have been widely used in the aerodynamics/aerospace community and there is an immense amount of literature, which has accumulated over two decades. This data however is focused on the details and subtleties specific to those engineering problems. In atmospheric sciences, the use of unstructured grids has been limited and considerable research is needed before the technology can mature. The objective of this research was to develop an alternative numerical scheme for modeling atmospheric flows on unstructured grids. The

following sections describe the implementation of a Godunov-type flow solver on an unstructured triangular mesh. The approximate Riemann solver used for calculating the advective fluxes, and the methodology for calculating subgrid scale diffusion on the unstructured mesh is described. Finally some benchmark analytic and idealized test cases are simulated for validation purposes.

2. Governing Equations

The basic equations of fluid flow comprise a set of partial differential equations for the conservation of mass, the conservation of momentum, the conservation of energy and an equation of state to close the system. The 2-D Navier-Stokes equations governing atmospheric flows (OOYAMA, 1990; MENDEZ-NÚÑEZ, 1993; KORAČIN, *et al.*, 1998), written in the conservative form are as follows:

$$\frac{\partial U}{\partial t}+\frac{\partial F}{\partial x}+\frac{\partial G}{\partial y}=Q+D \tag{1}$$

where,

$$U=\begin{bmatrix}\rho\\ \rho u\\ \rho v\\ \rho\theta\end{bmatrix},\quad F=\begin{bmatrix}\rho u\\ \rho u^2+p\\ \rho uv\\ \rho u\theta\end{bmatrix},\quad G=\begin{bmatrix}\rho v\\ \rho uv\\ \rho v^2+p\\ \rho v\theta\end{bmatrix} \tag{2}$$

ρ is the density of fluid, u is the velocity component in the x-direction, v is the velocity component in the y-direction and p is the pressure. If a parcel of air at temperature T and pressure p is subjected to an adiabatic compression or expansion to a final pressure of 10^5 Pa, then its potential temperature, θ, is given by:

$$\theta=T\left(\frac{p_0}{p}\right)^{R_d/c_p}. \tag{3}$$

In Equation (1), Q is the source term and D is the diffusive flux term defined by:

$$D=K\nabla^2 U. \tag{4}$$

In the momentum conservation equations, K is the subgrid scale eddy diffusivity coefficient of momentum ($= K_m$). In the conservation of energy equation, the Laplacian of potential temperature is multiplied by the eddy diffusivity coefficient of heat ($= K_h$).

The Smagorinsky-Lilly turbulence closure (LILLY, 1962; SMAGORINSKY, 1963) is used to parameterize the sub-grid scale diffusion in terms of the deformation tensor. The basic assumption is that the large (or resolved scales) lose energy by transferring it to the sub-grid scales (GATSKI *et al.,* 1996). This loss of energy from the large eddies is never recovered (i.e., it is dissipated). The eddy viscosity coefficient, K_m is related to the total deformation in terms of the Richardson number, Ri:

$$K_m = \begin{cases} \frac{(c\Delta)^2}{\sqrt{2}}|\mathrm{Def}|(1-Ri)^{0.5} & \text{if} \quad \mathrm{Ri} < 0.25 \\ 0 & \text{otherwise} \end{cases} \tag{5}$$

Total deformation rate Def is defined as:

$$\mathrm{Def}^2 = \frac{1}{2}\sum_i \sum_j D_{ij}^2. \tag{6}$$

The value of the Smagorinsky constant c is taken as 0.28 and Δ is the edge length. In two dimensions, Eq. (6) can be expanded as:

$$\mathrm{Def}^2 = \left(\frac{\partial u}{\partial x} - \frac{\partial v}{\partial y}\right)^2 + \left(\frac{\partial u}{\partial y} + \frac{\partial v}{\partial x}\right)^2 \tag{7}$$

where, $\left(\frac{\partial u}{\partial x} - \frac{\partial v}{\partial y}\right)$ is the stretching deformation and $\left(\frac{\partial u}{\partial y} + \frac{\partial v}{\partial x}\right)$ is the shearing deformation. In this study, for the sake of simplicity, the turbulent Prandtl number, Pr is set to unity:

$$\mathrm{Pr} = \frac{K_m}{K_h} = 1. \tag{8}$$

The source term Q, can be complex for atmospheric processes, and apart from body forces, may include terms for the heat sinks and sources produced due to the diurnal cycle of Earth, as well as microphysical processes of cloud formations and dissipations. For the purpose of this study, a simplified source term will be used. Atmosphere is assumed to be dry and the only source term is the gravitational force acting in the vertical direction. The system is closed by an equation of state for pressure,

$$p = C_0(\rho\theta)^{\gamma}, \tag{9}$$

where C_0 is a constant given by:

$$C_0 = \frac{R_d^{\gamma}}{p_0^{R_d/C_v}}. \tag{10}$$

In the above relations, γ is the ratio of specific heats ($= C_p/C_v = 1.4$), R_d is the gas constant for dry air ($= 287\ \mathrm{J\ K^{-1}\ kg^{-1}}$), p_0 is the base state pressure ($= 10^5$ Pa). C_p ($= 1004\ \mathrm{J\ K^{-1}\ kg^{-1}}$) and C_v ($= 717\ \mathrm{J\ K^{-1}\ kg^{-1}}$) are the specific heats of air at constant pressure and volume respectively.

3. Numerical Scheme

In the absence of turbulent diffusion, the Coriolis effect, body forces and other sink/source terms, the Navier-Stokes equations reduce to the well-known set of Euler equations. The 1-D Euler equations in the conservative form for an adiabatic atmosphere can be written as:

$$\frac{\partial U}{\partial t}+\frac{\partial F}{\partial x}=0, \tag{11}$$

where **U** is the vector of conserved variables:

$$U=\begin{bmatrix}u_1\\u_2\\u_3\end{bmatrix}\equiv\begin{bmatrix}\rho\\\rho u\\\rho\theta\end{bmatrix}, \tag{12}$$

and **F** is the flux vector,

$$F=\begin{bmatrix}f_1\\f_2\\f_3\end{bmatrix}\equiv\begin{bmatrix}\rho u\\\rho u^2+p\\\rho u\theta\end{bmatrix}. \tag{13}$$

The system is closed by an equation of state for pressure, Eqs. (9)–(10). The conservation laws in Eqs. (11)–(13) can be written in the discrete form as:

$$U_i^{n+1}=U_i^n+\frac{\Delta t}{\Delta x}\left[F_{i-1/2}+F_{i+1/2}\right], \tag{14}$$

bounded within a finite domain, $0 \leq x \leq L$, with appropriate initial and boundary conditions. Then, the Godunov flux is defined as,

$$F_{i+1/2}=F\left(U_{i+1/2}(0)\right), \tag{15}$$

where, $U_{i+\frac{1}{2}}(0)$ is the exact or approximate solution of the Riemann problem.

Godunov's method assumes piecewise constant data at cell centers. The Riemann problem is solved at each cell interface and the numerical flux is constructed from it. Thus, the global solution is a set of solutions of the local Riemann problems at each cell boundary (Fig. 1), which is then evolved in time.

a. The Harten-Lax-van Leer-Contact (HLLC) Approximate Riemann Solver

The approximate Riemann solver Harten-Lax-van Leer-Contact (HLLC) is an extension of the HLL (Harten, Lax, and van Leer) solver (HARTEN *et al.*, 1983) by TORO *et al.* (1994). In the original HLL Riemann approximation, the presence of contact discontinuities is neglected, which can results in errors in the presence of

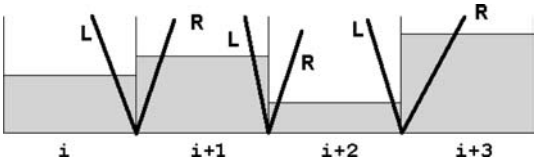

Figure 1
Piecewise constant data states within the computational cells. The discontinuities at cell boundaries form a set of local Riemann problems. L and R denote the waves on the left and the right side of the discontinuity, respectively.

shears within the flow. In Toro's extension (HLLC), the contact and shear waves are restored in the solution of the Riemann problem and it has the following three properties (LUO *et al.*, 2003):

- *Ability to resolve contact discontinuities and shear waves.*
- *Positivity preservation of scalar quantities.*
- *Enforcement of the entropy condition.*

The solver has been successfully implemented with both explicit and implicit time-marching schemes and used for calculations of Euler as well as the Navier-Stokes equations (BATTEN *et al.*, 1997; LUO *et al.*, 2003) for aerodynamics-related applications. The derivation of the HLLC flux is given in Appendix B. Here, the adaptation of the solver for Euler equations governing an adiabatic atmosphere is given. The flux at cell interface is defined as:

$$F^{\mathrm{HLLC}} = \begin{cases} F_L, & \text{if} \quad S_L > 0 \\ F_L^*, & \text{if} \quad S_L \le 0 < S_* \\ F_R^*, & \text{if} \quad S_* \le 0 \le S_R \\ F_R, & \text{if} \quad S_R < 0 \end{cases} \tag{16}$$

where, S_L, S_*, *and* S_R are the signal velocities associated with the three waves in the solution of the Riemann problem (the wave configuration in the HLLC approximate Riemann solver is shown in Fig. 2.). F_L and F_R flux vectors are given, respectively, by:

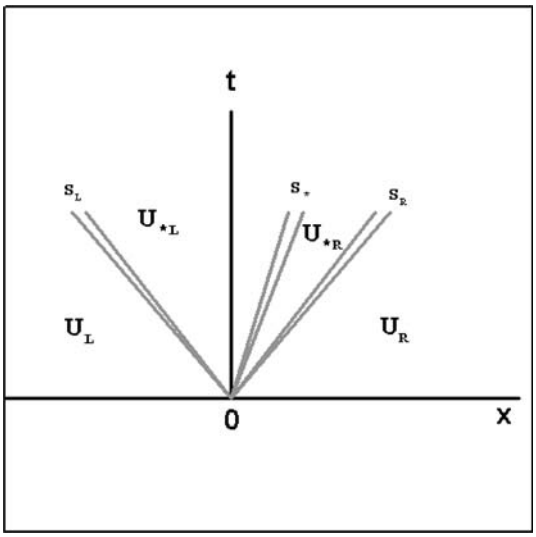

Figure 2
Wave configuration in the HLLC approximate Riemann solver. U_L is the data state to the left of the discontinuity, U_R is data state to the right of the discontinuity and U_* denotes the data state in the *starred* region (See Appendix B for details). S_L, S_* and S_R are the wave speeds associated with the three eigenvalues of the hyperbolic system.

$$F_L \equiv F(U_L) = \begin{pmatrix} (\rho u)_L \\ (\rho u^2)_L + p_L \\ (\rho\theta)_L \end{pmatrix}, \quad F_R \equiv F(U_R) = \begin{pmatrix} (\rho u)_R \\ (\rho u^2)_R + p_R \\ (\rho\theta)_R \end{pmatrix}. \tag{17}$$

The subscripts L and R denote the data states to the left and right of an interface (cell edge). The fluxes in the *starred* region are defined by:

$$F_L^* \equiv F(U_L^*) = \begin{pmatrix} S_*\rho_L^* \\ S_*(\rho u)_L^* + p_L^* \\ S_*(\rho\theta)_L^* \end{pmatrix}, \tag{18}$$

and,

$$F_R^* \equiv F(U_R^*) = \begin{pmatrix} S_*\rho_R^* \\ S_*(\rho u)_R^* + p_R^* \\ S_*(\rho\theta)_R^* \end{pmatrix}. \tag{19}$$

where,

$$U_L^* = \begin{pmatrix} \rho_L^* \\ (\rho u)_L^* \\ (\rho\theta)_L^* \end{pmatrix} = \frac{1}{S_L - S_*} \begin{pmatrix} (S_L - u_L)\rho_L \\ (S_L - u_L)(\rho u)_L + (p_L^* - p_L) \\ (S_L - u_L)(\rho\theta)_L \end{pmatrix}, \tag{20}$$

and,

$$U_R^* = \begin{pmatrix} \rho_R^* \\ (\rho u)_R^* \\ (\rho\theta)_R^* \end{pmatrix} = \frac{1}{S_R - S_*} \begin{pmatrix} (S_R - u_R)\rho_R \\ (S_R - u_R)(\rho u)_R + (p_R^* - p_R) \\ (S_R - u_R)(\rho\theta)_R \end{pmatrix}. \tag{21}$$

$p^*{}_L$ and $p^*{}_R$ are given by:

$$p_L^* = p_L + \rho_L(S_L - u_L)(S_* - u_L), \quad p_R^* = p_R + \rho_R(S_R - u_R)(S_* - u_R). \tag{22}$$

b. Calculation of Signal Velocities

The minimum and maximum signal velocities present in the solution of the Riemann problem can be estimated directly from the wave speeds, S_L and S_R:

$$S_L = u_L - a_L, \quad S_R = u_R + a_R. \tag{23}$$

The middle wave speed, S_*, is calculated using BATTEN's formulation (1997), by setting $p^*{}_L = p^*{}_R$:

$$S_* = \frac{\rho_R u_R(S_R - u_R) - \rho_L u_L(S_L - u_L) + p_L - p_R}{\rho_R(S_R - u_R) - \rho_L(S_L - u_L)}. \tag{24}$$

c. Diffusion Term

The diffusion term is calculated on the unstructured grid by using the method proposed by HOLMES and CONNELL (1989). Let,

$$L(U_i) = \sum_{k=1}^{n} w_{k,i}(U_k - U_i), \tag{25}$$

where, k represents the neighbors of cell i. The weights $w_{k,i}$ are chosen such that the pesudo-Laplacian of a linear function will be zero (as would be in the case of a true Laplacian).

$$w_{k,i} = 1 + \Delta w_{k,i}. \tag{26}$$

Since, linear functions have zero Laplacians,

$$L(x)_i = \sum_{k=1}^{n} w_k(x_k - x_i) = 0, \tag{27}$$

and,

$$L(y)_i = \sum_{k=1}^{n} w_k(y_k - y_i) = 0. \tag{28}$$

Defining the cost function, C as follows:

$$C = \sum_{k=1}^{n} (\Delta w_{k,i})^2. \tag{29}$$

This now becomes an optimization problem of minimizing the cost function in Eq. (29) given the constraints in Eqs. (27)–(28). Using Lagrange multipliers,

$$\Delta w_{k,i} = \lambda_x(x_k - x_i) + \lambda_y(y_k - y_i), \tag{30}$$

where,

$$\lambda_x = \frac{(I_{xy}R_y - I_{yy}R_x)}{(I_{xx}I_{yy} - I_{xy}^2)}; \quad \lambda_y = \frac{(I_{xy}R_x - I_{xx}R_y)}{(I_{xx}I_{yy} - I_{xy}^2)}, \tag{31}$$

and,

$$R_x = \sum_{k=1}^{n}(x_k - x_i); \quad R_y = \sum_{k=1}^{n}(y_k - y_i), \tag{32}$$

$$I_{xx} = \sum_{k=1}^{n}(x_k - x_i)^2; \quad I_{yy} = \sum_{k=1}^{n}(y_k - y_i)^2; \quad I_{xy}\sum_{k=1}^{n}(x_k - x_i)(y_k - y_i). \tag{33}$$

The geometric weights are calculated once at the beginning of the model run and stored in arrays. No special technique is needed for computing weights for the boundary cells. HOLMES and CONNELL (1989) report that for severely distorted meshes, these weights can deviate significantly from unity and suggest clipping the values within the range of (0,2).

d. Time-Marching

The solution is marched in time using Eq. (14) within a multi-stage explicit Runge-Kutta time marching scheme (JAMESON *et al.*, 1981). The scheme has relatively small memory requirements, is easy to implement and has been successfully used for obtaining both steady and unsteady solutions of the Euler as well as Navier-Stokes equations.

Let,

$$R_i \approx \frac{\partial U}{\partial t}. \tag{34}$$

Then the four-stage Runge-Kutta time-marching scheme can be written as:

$$\begin{aligned} U_i^{(0)} &= U_i^n \\ U_i^{(1)} &= U_i^{(0)} - \alpha_1 \Delta t R_i^{(0)} \\ U_i^{(2)} &= U_i^{(0)} - \alpha_2 \Delta t R_i^{(1)} \\ U_i^{(3)} &= U_i^{(0)} - \alpha_3 \Delta t R_i^{(2)} \\ U_i^{(4)} &= U_i^{(0)} - \alpha_4 \Delta t R_i^{(3)} \\ U_i^{n+1} &= U_i^{(4)} \end{aligned} \tag{35}$$

where, $\alpha_1 = 1/4, \alpha_2 = 1/3, \alpha_3 = 1/2$ and $\alpha_4 = 1$, are the Runge-Kutta constants. During the time integration, the local Riemann solution on one interface should not be allowed to interfere with the Riemann solution on another interface. If the interference of waves occurs, then the solution of the Riemann problem can no longer be considered local. This forms the basis of the Courant restriction on the Godunov method. The time step is calculated by finding the maximum wave speed in each cell:

$$\Delta t = CFL \frac{\Delta x}{\mathrm{abs}(u + a)}, \tag{36}$$

where, u is the normal velocity at edge and Δx is the distance between the cell center and the point of intersection of the edge with the line connecting the cell centers on either side of the edge. The minimum of the time steps in each cell is used for marching the solution forward in time.

e. Implementation on Unstructured Grids

The implementation of the flow solver on an unstructured triangular grid for the scalar transport equation was described in detail in the first part (AHMAD *et al.*, 2006). The methodology is briefly summarized in this section. The scheme uses cell-centered control volumes. The advective fluxes are calculated by summing all the incoming and outgoing fluxes through each face of the control volume. The flux across each edge of the cell is calculated using the HLLC approximate Riemann solver. The values on either side of a cell edge form the initial conditions for the Riemann problem. The solution is marched in time within the multi-stage Runge-Kutta explicit time marching scheme (JAMESON *et al.*, 1981). In a loop over edges, the values of cells on either side of the edge are used to calculate the fluxes. Once the fluxes have been calculated they are added to the cell centered value in a loop over cells (Fig. 3). For the second-order calculation, gradient-limited extrapolated values are used in the Riemann solver instead of cell averages (VAN LEER, 1979). Both the Green-Gauss and the Linear Least-Squares gradient reconstruction (BARTH and JESPERSON, 1989) techniques have been implemented to extend the spatial accuracy of the scheme to higher-order. The scheme is made *total variation diminishing* (HARTEN, 1983) with the help of slope limiters (BARTH and JESPERSON, 1989; VAN LEER, 1979). The limiting procedure is performed on conserved variables ($\rho, \rho u, \rho v,$ and $\rho\theta$). No explicit filtering is required for the stability of the numerical scheme.

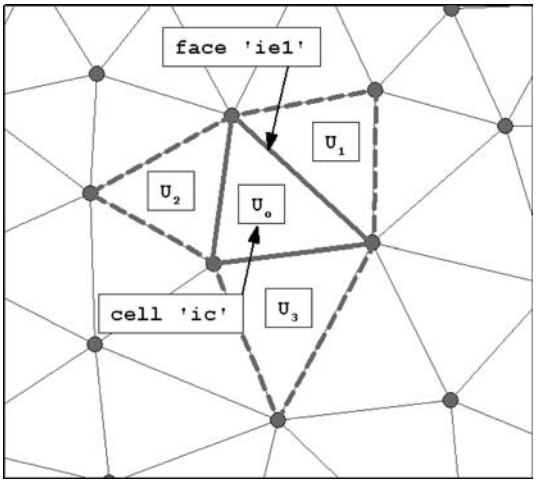

Figure 3
In a loop over edges the cell values on either side of the face/edge are used by the Riemann solver to calculate fluxes. Then in a loop over cells the fluxes are added to update the cell centered values. U_0 represents the data state in cell '**ic**' and U_1, U_2, and U_3 are the data states (conserved quantities) in the neighboring cells.

f. Boundary Conditions

Implementation of lateral boundary conditions (inflow/outflow) is straightforward. The boundary conditions are stored in *ghost* cells at model initialization. The *ghost* cells are reflections of the boundary cells (Fig. 4). The Riemann solver then uses these values for calculating fluxes across boundary edges. For an inflow boundary condition, the values are prescribed in the *ghost* cells and for outflow the values from the boundary cells are assigned to the *ghost* cells. LEVEQUE (2002) describes in detail the implementation of boundary conditions for hyperbolic conservation laws.

g. Solver Steps

The solution algorithm for constructing Godunov-type schemes *via* the HLLC Riemann solver can be summarized as follows:

1. Given the left and the right data states across each cell face/edge, calculate the signal velocities, $S_{L,}$, S_*, and S_R associated with the waves present in the solution of the Reimann Problem by Eqs. (23) *and* (24).
2. Construct the Godunov flux obtained from the HLLC approximate Riemann solver using Eqs. (16)–(22), depending on the magnitude of signal velocities.
3. Add gravity and subgrid scale diffusion as source terms at the cell centers. Different methodologies to include source terms (LEVEQUE, 2002; BOTTA *et al.*, 2004) can be used.
4. Evolve the set of conservative variables explicitly in time using Eqs. (34)–(35).

4. Results

In this section, the results from two different test cases are presented — Sod shock tube case, which is essentially a one-dimensional problem is simulated on a 2-D

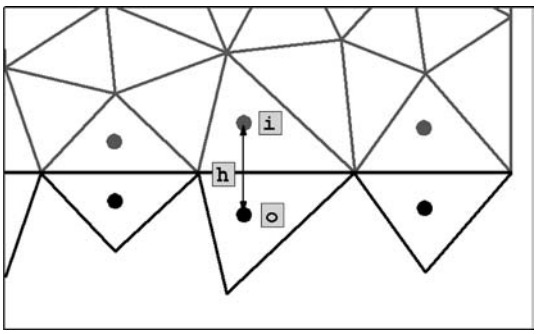

Figure 4
Boundary (outer/ghost) cells are reflections of interior cells. In the Figure "**i**" represents the interior or boundary cell and "**o**" represents an outer or ghost cell.

unstructured triangular mesh and compared with the exact solution. The convection of a warm bubble in a neutral atmosphere is simulated for the second test case by solving the complete Navier-Stokes equations on an unstructured triangular mesh.

a. Euler Solution: Shock Tube

The HLLC solver for atmospheric flows was evaluated against benchmark cases of the Riemann problem with exact solutions. The Sod shock tube (SOD, 1978) test

Table 1

Initial conditions for the shock tube test cases

Case	Mach Number	Density $(kg/m^3)r_{left}$	Density $(kg/m^3)r_{right}$	Velocity $(m/s)u_{left}$	Velocity $(m/s)u_{right}$	Pressure $(Pa)p_{left}$	Pressure $(Pa)p_{right}$
1	0.21	1.0	0.4	0	0	1.0	0.6
2	0.90	1.0	0.125	0	0	1.0	0.1

The subscript ''left'' denotes the data state on the left side of discontinuity and the subscript ''right'' denotes the data state on the right side of the discontinuity.

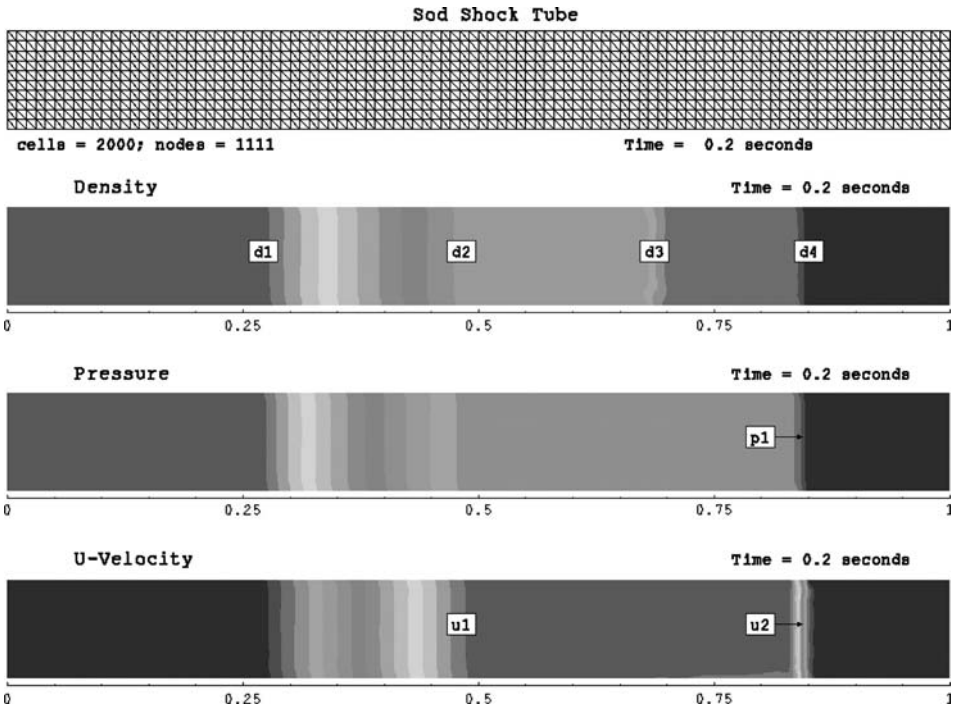

Figure 5

Sod Shock Tube. From top to bottom: the computational mesh, density (kg/m^3), pressure (Pa) and the u-velocity (m/s) in the tube at time = 0.2 seconds.

case is described in this section. The initial conditions (density, velocity, and pressure) are given in Table 1. The mesh used for the simulation is shown in Figure 5 (top panel). The higher-order solution for Case 2 is also shown in Figure 5. The different wave structures admitted by the equation set have been resolved and can be seen in the plots of density, pressure and velocity. The expansion (left propagating rarefaction wave), e.g., can be seen between point *d1* and point *d2* in the density plot (Figure 5). The contact discontinuity lies between point *d2* and point *d3* and the shock front is resolved at point *d4*. In the pressure plot, *e.g.*, the sudden drop across the shock wave (point *p1*) can be seen. The velocity plot shows the rarefaction wave (the slope left of point *u1*) as the gas expands and the shock front propagates to the right (point *u2*). MENDEZ-NÚÑEZ and CARROLL (1993) have also compared different numerical schemes (Leapfrog, MacCormack and MPDATA) for simulating the compressible atmospheric equation set with different shock tube cases (TAYLOR *et al.*, 1972). The results of MENDEZ-NÚÑEZ and CAROLL (1993) show that the Gibbs oscillations contaminate the solution obtained by all three schemes. Unlike the current schemes used in atmospheric modeling, there are minimal dispersion errors introduced in the solution by the Godunov scheme and its higher-order extension.

Figures 6–8 show the comparison of the first-order Godunov scheme and its higher-order extension *via* MUSCL with the exact solution for two different test cases. The first case is a modified Sod shock tube case in which the initial data is adjusted to give a low Mach number ($\sim$0.2), whereas the second test case gives a Mach number of 0.9. The low Mach number solution is in good agreement with the exact solution for all three quantities (density, pressure and velocity). The density for the high Mach number case however is overestimated behind the shock front in both the first-order Godunov solution and its higher-order extension via MUSCL (Fig. 6). The velocity field is overestimated by the higher-order extension (Fig. 7). It should be noted that Eqs. (11)–(13) are based on the assumption that the processes in the atmosphere are adiabatic. Although the eigenspace of Eqs. (11)–(13) admits shock waves in a mathematical sense (see Appendix A), physically it is known that isentropic/adiabatic processes do not admit strong shocks. For simulating atmospheric flows, however, this is not an issue. The development of a high-resolution Godunov-type method is intended to resolve atmospheric flows characterized by steep gradients (fronts, drylines, tornadoes, hurricanes, etc.) and not shock waves (blasts, explosions, etc.). Furthermore, atmospheric flows in general are low Mach number variable density flows.

b. Navier-Stokes Solution: Kelvin-Helmholtz Instability

The convection in neutral atmosphere is a popular test case for validating numerical schemes for atmospheric flow simulations (e.g., REISNER *et al.*, 2003; KORAČIN *et al.*, 1998). In the absence of an analytical solution, the test can evaluate the scheme only in qualitative terms. This evaluation however, provides valuable

information on the scheme's ability to simulate the fundamentals of atmospheric thermodynamics and dynamics. The set of Navier-Stokes equations in two dimensions was solved for this problem. Model was initialized by introducing a warm bubble with a diameter of 500 m and a constant potential temperature of 0.5 degrees higher than the surrounding environment (neutral atmosphere in hydrostatic balance with a uniform potential temperature of 300 K). A 1 km $\times$ 1 km domain was defined for the simulation. The pressure was re-adjusted for hydrostatic equilibrium after the introduction of the thermal. The variables were first initialized on a structured grid and then interpolated to the unstructured mesh using bilinear

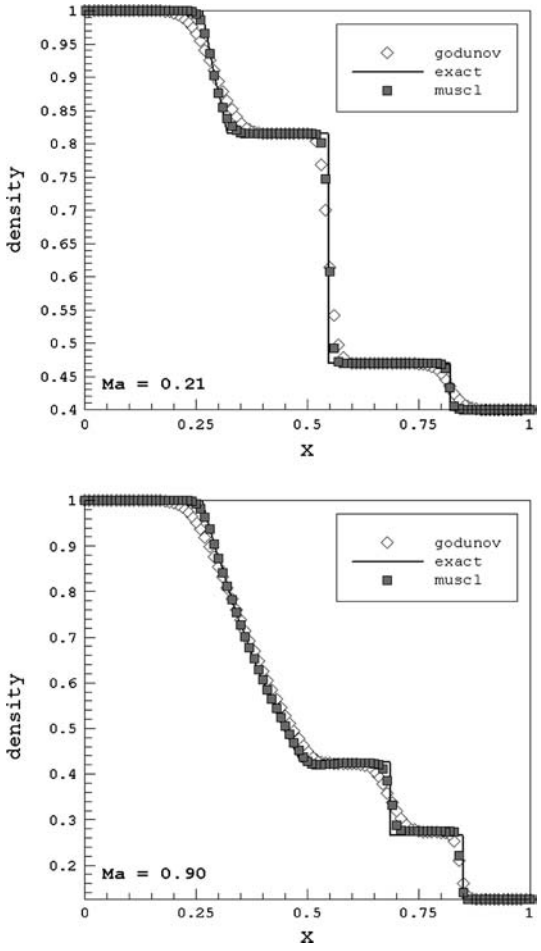

Figure 6
Shock Tube. Density (kg/m^3) for Test 1 (Ma = 0.21) is shown in the top panel and for Test 2 (Ma = 0.9) in the bottom panel. Time = 0.2 seconds. The centerline data of the shock tube (Fig. 5) from $x = 0$ to $x = 1$ m is plotted.

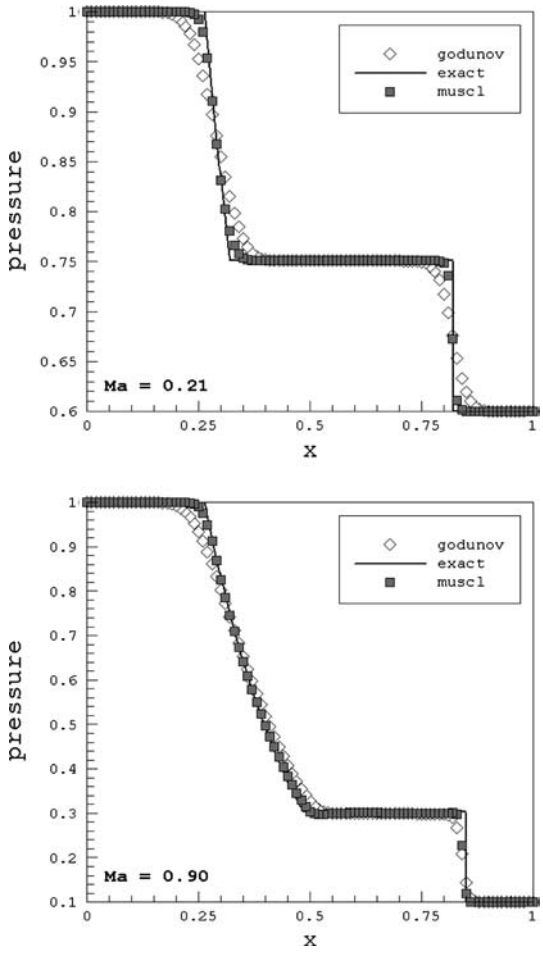

Figure 7
Shock Tube. Pressure (Pa) for Test 1 (Ma = 0.21) is shown in the top panel and for Test 2 (Ma = 0.9) in the bottom panel. Time = 0.2 seconds. The centerline data of the shock tube (Fig. 5) from $x = 0$ to $x = 1$ m is plotted.

interpolation. It should be noted that initializing a perfect hydrostatic balance on an unstructured mesh is nontrivial and the interpolation from the structured grid to the unstructured grid introduces errors in the initial conditions (i.e., hydrostatic imbalances in the initial state of the atmosphere). All domain boundaries were treated as solid walls. The unstructured triangular mesh consisted of 39386 triangular elements with edge lengths varying from 3.5 m to 12.4 m.

Shear is generated due to gradients in the flow normal to its direction and often results in instabilities. In stratified fluids (e.g., the atmosphere) the instabilities due to shear are damped out by the stratification. The Miles theorem predicts the transition

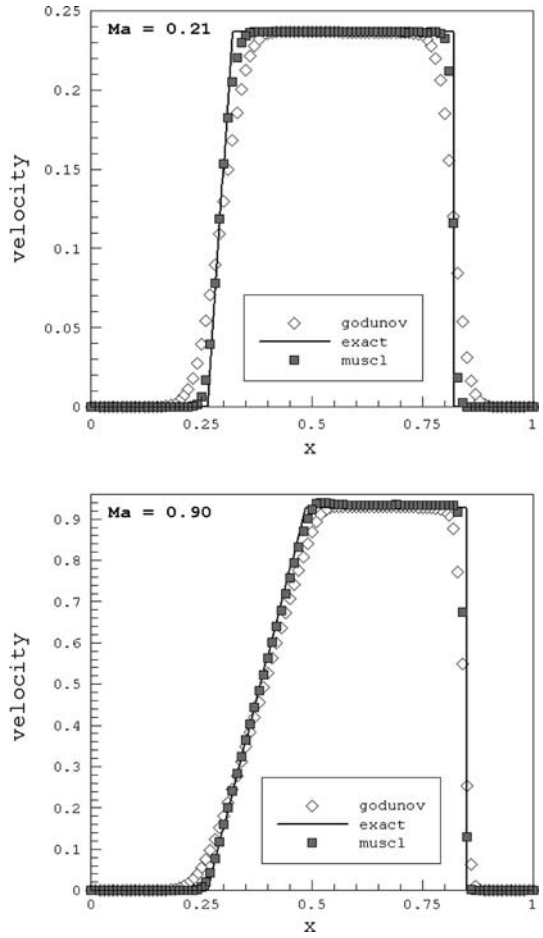

Figure 8
Shock Tube. Velocity (m/s) for Test 1 (Ma = 0.21) is shown in the top panel and for Test 2 (Ma = 0.9) in the bottom panel. Time = 0.2 seconds. The centerline data of the shock tube (Fig. 5) from $x = 0$ to $x = 1$ m is plotted.

from stable to unstable flow and the onset of the Kelvin-Helmholtz instability for low Richardson numbers (Ri < 0.25). The Kelvin-Helmholtz type of instability is common in the atmosphere and has been observed in billow clouds. The breaking of waves in the Kelvin-Helmholtz instability can generate the clear air turbulence (CAT) in the atmosphere.

The objective of this model validation run was to simulate the onset of the Kelvin-Helmholtz type of instability in the atmosphere. Buoyant thermals are highly nonlinear phenomena and therefore, the detailed structure of the evolving thermal is dependent on the type of mathematical model used, i.e., the equation set used — compressible, quasi-compressible, anelastic, etc. (CARPENTER *et al.*, 1990; MENDEZ-

NÚÑEZ and CARROLL, 1994). Nonetheless, there are certain features which are expected in the resulting flow field. The introduction of the thermal in the domain generates acceleration in the center of the bubble accompanied by downdrafts on either side of the bubble. As the buoyant thermal rises, a shear layer is developed at the lateral edges of the thermal. Initially the atmosphere is strongly stratified which damps out the onset of flow instabilities, but as the thermal rises, the weakening of stratification at the edge of the thermal triggers the onset of the instability. Figures 9–11 show the time evolution of potential temperature gradient, shear, the Richardson number (scaled from –0.26 to 0.26; the values greater than 0.26 are set to zero) and potential temperature. The generation of a shear layer and weakening of stratification resulting in the Kelvin-Helmholtz type of instability can be seen in the figures. The vectors in the figures represent only the flow direction.

5. *Discussion*

In the case of complex computational domains, either the finite volume or finite-element schemes are usually used, instead of finite-difference schemes. In the context of atmospheric modeling, the accurate discretization of the underlying terrain and shoreline features becomes important for meso- and micro-scale flows. For urban-scale flows, in which individual buildings have to be explicitly resolved, a finite-difference type scheme would be extremely cumbersome if not impossible to implement. The Godunov-type scheme described in this paper is a finite volume scheme; therefore, it can be used to discretize complex geometries. Although the basic element for a control volume used in this study is a triangle, the scheme can easily be extended to other types of polyhedral elements.

The scheme is conservative and shows minimal dispersion and diffusion errors. No grid staggering is required for stability, which makes the implementation of the scheme somewhat simpler. All variables are stored at cell centers. No explicit diffusion/filtering is needed to maintain the stability of the scheme. The scheme also ensures the positivity of scalar quantities. This property becomes important when the simulation includes the transport of microphysical quantities. Some of these advantages of Godunov-type schemes have been demonstrated in earlier works. For the scalar transport equation, the reader can refer to the work of CARPENTER *et al.* (1990). The results of the present study (Euler equations) can be compared with the data reported by MENDEZ-NÚÑEZ and CAROLL (1993). The results of MENDEZ-NÚÑEZ and CAROLL (1993) show that the Gibbs oscillations contaminate the solution obtained by the Leapfrog, MacCormack and MPDATA schemes. Unlike the current schemes used in atmospheric modeling, there are minimal dispersion errors introduced in the solution by the Godunov scheme and its higher-order extension.

Although the scheme is able to simulate the basics of atmospheric dynamics and thermodynamics as shown in the simulation of the buoyant thermal, its ability to

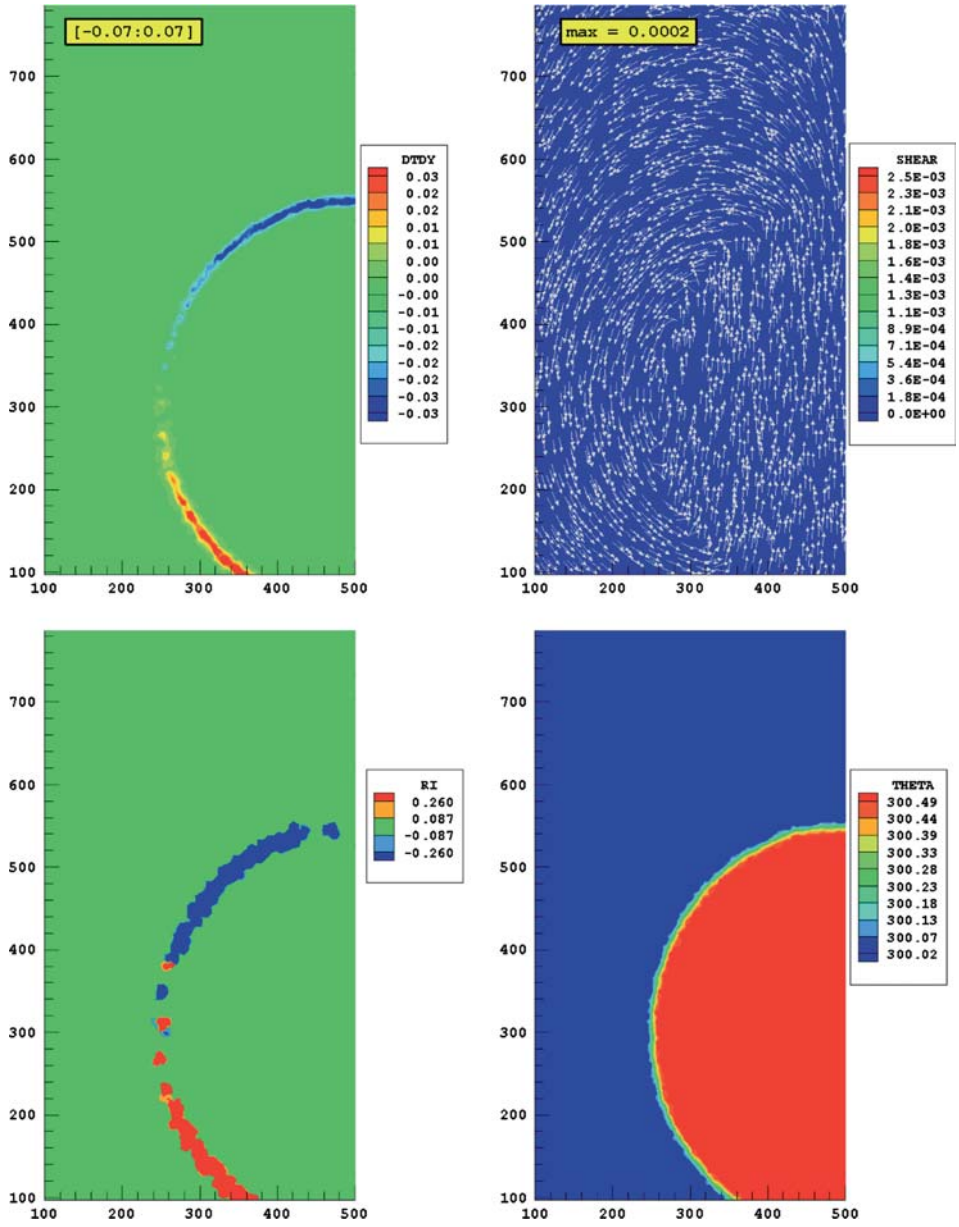

Figure 9
Potential temperature gradient (K/m) (top left), shear (1/s) (top right), Richardson number (bottom left) and potential temperature (K) (bottom right). Time = 14 s.

simulate more complex atmospheric flows which include the diurnal variation and microphysical processes has yet to be tested. This needs to be addressed in future extensions of the numerical scheme.

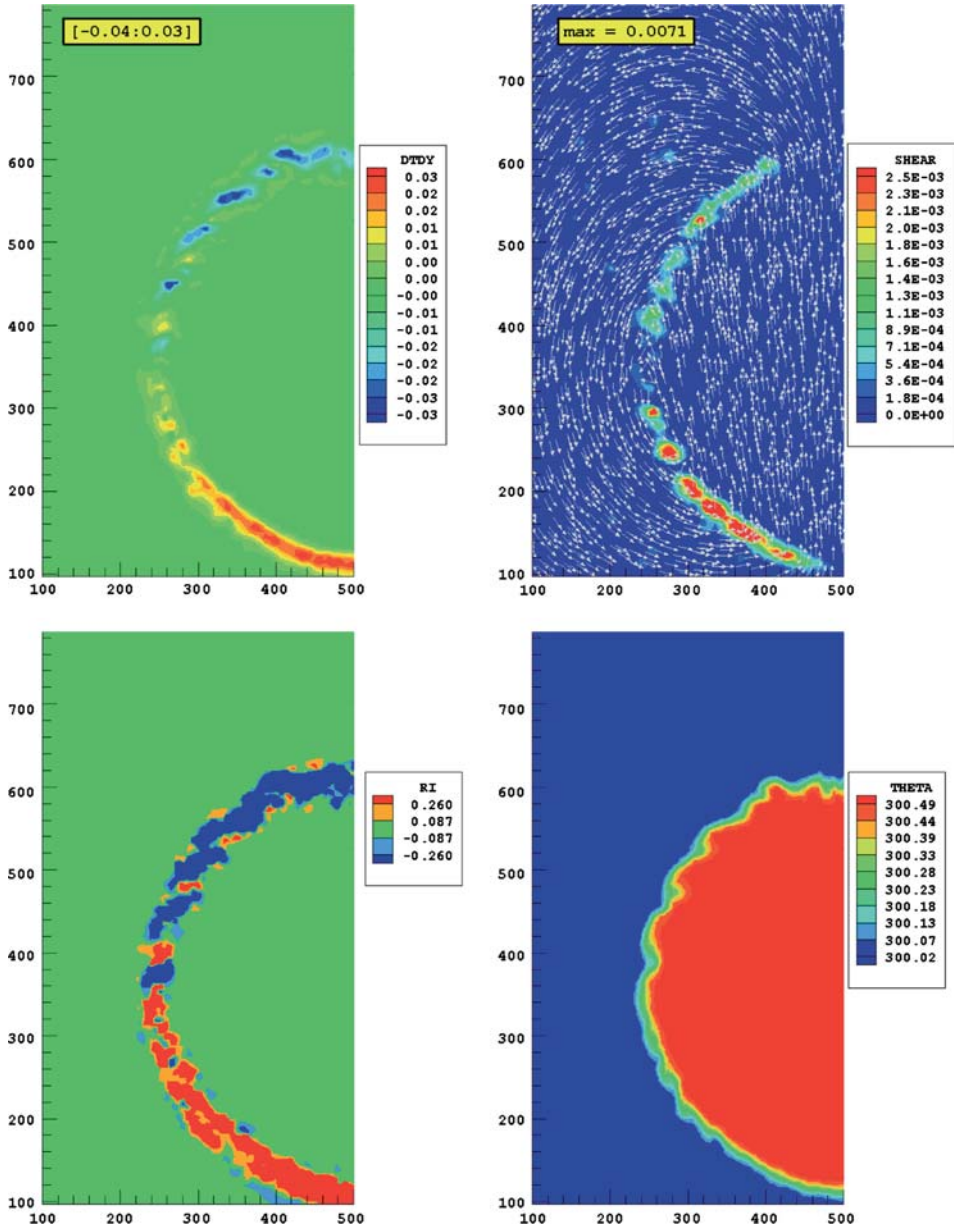

Figure 10
Potential temperature gradient (K/m) (top left), shear (1/s) (top right), Richardson number (bottom left) and potential temperature (K) (bottom right). Time = 145 s.

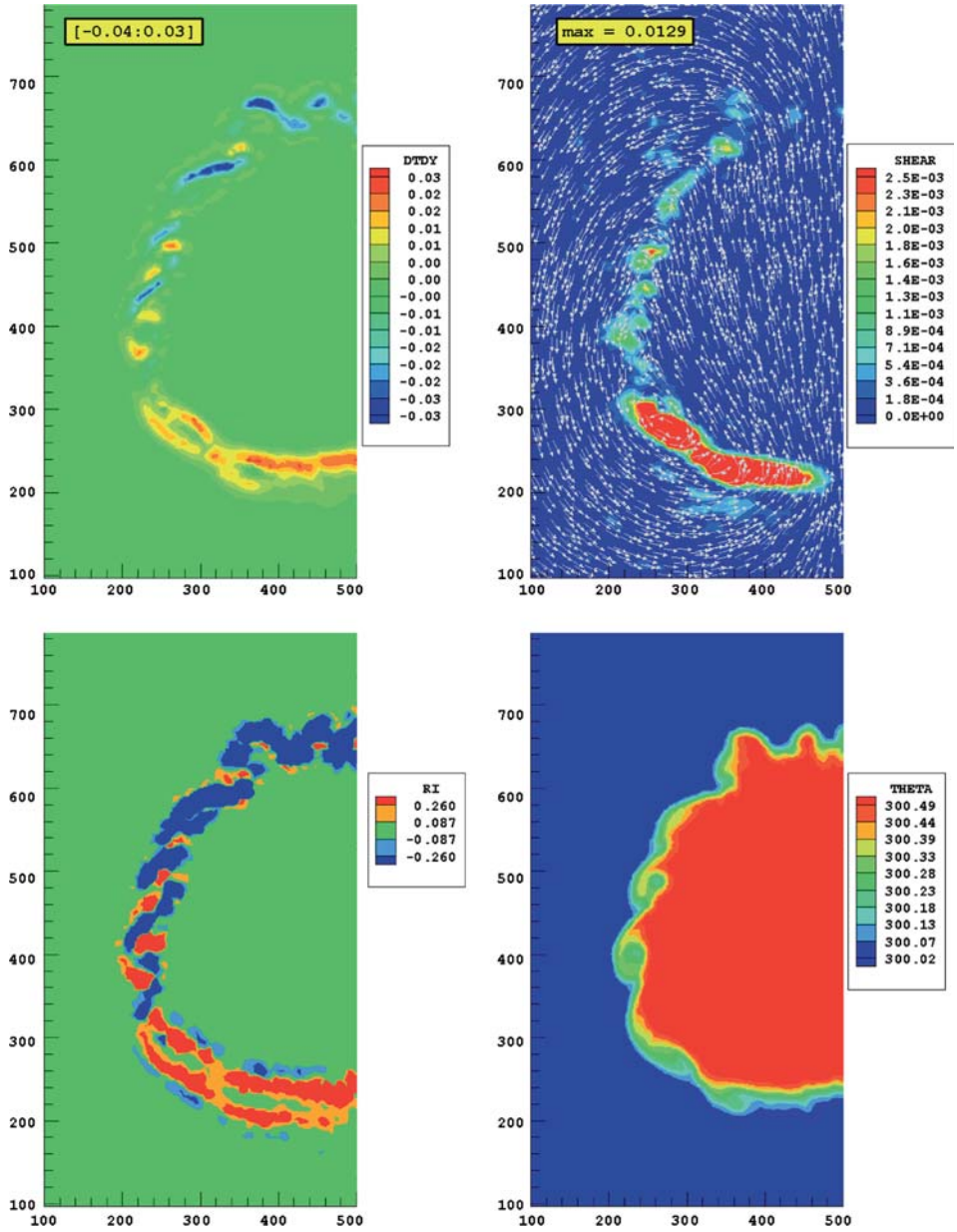

Figure 11
Potential temperature gradient (K/m) (top left), shear (1/s) (top right), Richardson number (bottom left) and potential temperature (K) (bottom right). Time = 217 s.

6. Conclusions

This work has opened up the door for future use of high-resolution Godunov-type methods for atmospheric flow simulations on unstructured meshes. The main results of this study can be summarized as follows:

- The comparison with exact solutions showed that the scheme could resolve the different types of wave structures admitted by the atmospheric flow equation set.
- The scheme is conservative and requires no special grid staggering or explicit filtering for stability. There are minimal dispersion errors which are usually associated with centered finite difference schemes.
- The proposed scheme was able to simulate the onset of Kelvin-Helmholtz type instability and shows promise in simulating flows characterized by steep gradients on the meso- micro- and urban-scales. Centered finite-difference schemes require explicit filtering for stability in regions of steep gradients to damp out spurious oscillations.
- The positivity of scalars is ensured by the flow solver (an important property when considering the transport of microphysical quantities).
- The use of unstructured grids provides the ability to simulate the complex, multi-scale atmospheric flows in a computationally efficient manner. The implentation of solution-adaptive techniques is also relatively simpler.

The use of unstructured grids in the atmospheric modeling community is relatively new and more research is needed for the technology to mature for atmospheric applications. The future extensions of this work will focus on better CPU performance provided by implementing an implicit time-marching scheme (LUO *et al.*, 1998) that can further increase the robustness of the flow solver. Although an edge-based data structure is used for computational efficiency in the current study — issues related to code optimization in terms of grid data structures, which minimize cache misses, also need to be addressed. Inclusion of more physics (microphysics, radiation schemes and surface layer physics) is needed for simulating realistic flows.

Acknowledgements

Many thanks to Drs. Hong Luo and Mary Hall for helpful discussions and suggestions regarding the subject. We would also like to thank the reviewers for comments which enhanced the manuscript.

Appendix A

Godunov's method and its higher-order extensions have been designed for hyperbolic conservation laws. It is shown that the set of one-dimensional Euler

equations governing the atmospheric flow are hyperbolic and thus an attempt can be made to apply the family of high-resolution numerical methods which have been developed specifically for solving hyperbolic conservation laws. The Euler equations are written in a quasi-linear form,

$$U_t + A(U)U_x = 0. \tag{A.1}$$

The subscripts t and x denote derivatives in time and space respectively, and **A(U)** is the Jacobian matrix defined as,

$$\mathbf{A}(\mathbf{U}) = \begin{bmatrix} \frac{\partial f_1}{\partial u_1} & \frac{\partial f_1}{\partial u_2} & \frac{\partial f_1}{\partial u_3} \\ \frac{\partial f_2}{\partial u_1} & \frac{\partial f_2}{\partial u_2} & \frac{\partial f_2}{\partial u_3} \\ \frac{\partial f_3}{\partial u_1} & \frac{\partial f_3}{\partial u_2} & \frac{\partial f_3}{\partial u_3} \end{bmatrix}. \tag{A.2}$$

The Jacobian matrix can be found by expressing the components of the flux vector **F** in terms of the components of the **U** vector of conserved variables:

$$\mathbf{F}(\mathbf{U}) = \begin{bmatrix} u_2 \\ \frac{u_2^2}{u_1} + C_o u_3^{\gamma} \\ \frac{u_2 u_3}{u_1} \end{bmatrix}. \tag{A.3}$$

After some algebraic manipulations, the matrix in Eq. (A.2) simplifies to:

$$\mathbf{A}(\mathbf{U}) = \begin{bmatrix} 0 & 1 & 0 \\ -u^2 & 2u & a^2/\theta \\ -u\theta & \theta & u \end{bmatrix}, \tag{A.4}$$

where, a is the speed of sound.

Proposition 1: *The one-dimensional Euler equations governing the atmospheric flows are hyperbolic.*

Proof. The eigenvalues of the Jacobian matrix **A(U)** are found by setting,

$$|A(U) - \lambda I| = 0, \tag{A.5}$$

where, λ_i are the eigenvalues and **I** is the identity matrix. The solution of the resulting polynomial gives the following eigenvalues:

$$\lambda = \begin{bmatrix} u - a \\ u \\ u + a \end{bmatrix}. \tag{A.6}$$

Since all eigenvalues are real, the system is hyperbolic.

Proposition 2: *The K^2 characteristic field is linearly degenerate and the K^1 and K^3 characteristic fields are genuinely nonlinear.*

The right eigenvectors of the system can be derived by solving for:

$$K = [\, k_1 \quad k_2 \quad k_3 \,]^T \tag{A.7}$$

such that,

$$AK = \lambda K \tag{A.8}$$

The right eigenvectors of the system are:

$$K^1 = \begin{bmatrix} 1 \\ u - a \\ \theta \end{bmatrix}; \quad K^2 = \begin{bmatrix} 1 \\ u \\ 0 \end{bmatrix}; \quad K^3 = \begin{bmatrix} 1 \\ u + a \\ \theta \end{bmatrix}. \tag{A.9}$$

Proof. Since,

$$\nabla\lambda_1(U) \cdot K^1 \neq 0; \quad \nabla\lambda_2(U) \cdot K^2 = 0; \quad \nabla\lambda_3(U) \cdot K^3 \neq 0. \tag{A.10}$$

It follows that the K^2 characteristic field is *linearly degenerate* which implies that the wave associated with it is a *contact discontinuity,* whereas the *genuinely nonlinear* K^1 and K^3 fields will have waves, which can either be *rarefactions* (smooth waves) or *shocks* (discontinuities).

Appendix B

In the HLLC Riemann solver the intercell fluxes are computed directly (Toro, 1999). It is assumed that the wave speeds separating the different constant states are known, then a closed-form approximation for the flux can be derived by integrating the conservation laws.

Given a system of hyperbolic conservation laws:

$$U_t + F(U)_x = 0 \tag{B.1}$$

and a discontinuous wave solution of speed S_i associated with the λ_i-characteristic field, the Rankine-Hugoniot Conditions state:

$$\Delta F = S_i \Delta U. \tag{B.2}$$

The wave configuration assumes the presence of the slowest (S_L) and the fastest (S_R) signal speeds and includes a middle wave speed S_*, corresponding to the eigenvalue associated with the K_2-characteristic field ($\lambda_2 = u$). Applying the Rankine-Hugoniot Conditions across the three waves yields the following relations:

$$\begin{aligned} F_L^* &= F_L + S_L\left(U_L^* - U_L\right) \\ F_R^* &= F_L^* + S_*\left(U_R^* - U_L^*\right) \\ F_R^* &= F_R + S_R\left(U_R^* - U_R\right) \end{aligned} \tag{B.3}$$

The subscripts L and R denote the data states on the left and right of a cell interface respectively. There are four unknowns and three equations. The aim is to find $U^*{}_L$ and $U^*{}_R$ so that $F^*{}_L$ and $F^*{}_R$ can be determined. The following conditions are imposed on the Riemann solver:

$$\begin{aligned} u_{*L} = u_{*R} = u_* = S_* \\ p_{*L} = p_{*R} = p_* \end{aligned} \tag{B.4}$$

Equation (B.3) can now be solved for $U^*{}_L$ and $U^*{}_R$:

$$U_L^* = \begin{pmatrix} \rho_L^* \\ (\rho u)_L^* \\ (\rho\theta)_L^* \end{pmatrix} = \frac{1}{S_L - S_*} \begin{pmatrix} (S_L - u_L)\rho_L \\ (S_L - u_L)(\rho u)_L + (p_L^* - p_L) \\ (S_L - u_L)(\rho\theta)_L \end{pmatrix}, \tag{B.5}$$

and,

$$U_R^* = \begin{pmatrix} \rho_R^* \\ (\rho u)_R^* \\ (\rho\theta)_R^* \end{pmatrix} = \frac{1}{S_R - S_*} \begin{pmatrix} (S_R - u_R)\rho_R \\ (S_R - u_R)(\rho u)_R + (p_R^* - p_R) \\ (S_R - u_R)(\rho\theta)_R \end{pmatrix}. \tag{B.6}$$

Using the values $U^*{}_L$ and $U^*{}_R$ of in Eq. (B.3) gives the relations for fluxes ($F^*{}_L$ and $F^*{}_R$) in the star region:

$$F_L \equiv F(U_L) = \begin{pmatrix} (\rho u)_L \\ (\rho u^2)_L + p_L \\ (\rho\theta)_L \end{pmatrix}, \quad F_R \equiv F(U_R) = \begin{pmatrix} (\rho u)_R \\ (\rho u^2)_R + p_R \\ (\rho\theta)_R \end{pmatrix}. \tag{B.7}$$

The states to the left and the right of the starred region are already known. The F_L and F_R flux vectors are given by:

$$F_L \equiv F(U_L) = \begin{pmatrix} (\rho u)_L \\ (\rho u^2)_L + p_L \\ (\rho\theta)_L \end{pmatrix}, \quad F_R \equiv F(U_R) = \begin{pmatrix} (\rho u)_R \\ (\rho u^2)_R + p_R \\ (\rho\theta)_R \end{pmatrix}. \tag{B.8}$$

The subscripts L and R denote the data states to the left and right of an interface (cell edge). The complete HLLC flux can now be written as:

$$F^{\mathrm{HLLC}} = \begin{cases} F_L, & \text{if} \quad S_L > 0 \\ F_L^*, & \text{if} \quad S_L \le 0 < S_* \\ F_R^*, & \text{if} \quad S_* \le 0 \le S_R \\ F_R, & \text{if} \quad S_R < 0 \end{cases} \tag{B.9}$$

where, S_L, S_*, *and* S_R are the signal velocities associated with the three waves in the solution of the Riemann problem. The minimum and maximum signal velocities present in the solution of the Riemann problem can be estimated directly from the wave speeds, S_L and S_R:

$$S_L = u_L - a_L \quad S_R = u_R + a_R. \tag{B.10}$$

Once the minimum and maximum signal velocities are known, applying conditions in Eq. (B.4) to the Rankine-Hugonoit relations in Equation (B.3) gives the relations for pressures (p^*_L and p^*_R):

$$p^*_L = p_L + \rho_L(S_L - u_L)(S_* - u_L), \quad p^*_R = p_R + \rho_R(S_R - u_R)(S_* - u_R). \tag{B.11}$$

The middle wave speed, S_*, was calculated by using setting $p^*_L = p^*_R$:

$$S_* = \frac{\rho_R u_R(S_R - u_R) - \rho_L u_L(S_L - u_L) + p_L - p_R}{\rho_R(S_R - u_R) - \rho_L(S_L - u_L)} \tag{B.12}$$

Appendix C

The definitions and units of symbols used in the text are listed here for reference:

a	speed of sound (m/s)
c	Smagorinsky constant
CFL	Courant-Friedrich-Lewis number
c_p	specific heat of dry air at constant pressure ($JK^{-1}kg^{-1}$)
c_v	specific heat of dry air at constant volume ($JK^{-1}kg^{-1}$)
Def	total deformation
D_{ij}	deformation tensor
F	flux vector of conserved quantities in x-direction
F_L	flux on the left of the interface (kg/m^2s)
F_R	flux on the right of the interface (kg/m^2s)
$F^*_{L,R}$	fluxes in the starred region (kg/m^2s)
G	flux vector of conserved quantities in y-direction
K_h	eddy diffusivity coefficient of heat (m^2/s)
K_m	eddy diffusivity coefficient of momentum (m^2/s)
K^i	Characteristic fields associated with λ_I eigenvalues
Ma	Mach number
P	pressure (Pa)
p_o	base state (reference) pressure = 10^5 Pa
Pr	Prandtl number
R_d	gas constant for dry air ($JK^{-1}kg^{-1}$)
Ri	Richardson number
S_L	signal velocity associated with the wave on the left of the interface (m/s)
S_R	signal velocity associated with the wave on the right of the interface (m/s)
S_*	signal velocity associated with the wave in the starred region (m/s)
U	vector of conserved quantities
u	velocity in x-direction (m/s)
v	velocity in y-direction (m/s)
α_i	Runge-Kutta constants
Δt	time step (s)
Δx	mesh resolution (m)
γ	ratio of specific heats
ρ	fluid density (kg/m^3)
λ_i	Eigenvalues of the hyperbolic system
θ	potential temperature (K)

References

Ahmad, N., Boybeyi, Z., Löhner, R., and Sarma, A. 2006, *A Godunov-type scheme for atmospheric flows on unstructured grids: Scalar transport*, Pure Appl. Geophys. *163*(8), 1699–1735.

Ahmad, N., Bacon, D., Hall, M., and Sarma, A. 2006, *Application of the Multi-Dimensional Positive Definite Advection Transport Algorithm (MPDATA) to environmental modeling on adaptive unstructured grids,* Int. J. Num. Meth. Fluids *50*(10), 1247–1268.

Bacon, D. P., Ahmad, N. N., Boybeyi, Z., Dunn, T. J., Hall, M. S., Lee, P. C. S., Sarma, R. A., Turner, M. D., Waight, K., Young, S., and Zack, J. (2000), A d*ynamically adapting weather and dispersion model: The operational multiscale environment model with grid adaptivity (OMEGA),* Monthly Weather Rev. *128*, 2044–2076.

Barth, T. J. and Jesperson, D. C. (1989), *The design and application of upwind schemes on unstructured meshes,* AIAA Paper 1989–0366.

Batten, P., Leschziner, M. A., and Goldberg, U. C. (1997), *Average-state Jacobians and implicit methods for compressible viscous and turbulent flows,* J. Comput. Phys. *137*, 38–78.

Boris, J. and Book, D. L. (1973), *Flux-corrected transport. I. SHASTA, A fluid transport algorithm that works,* J. Comput. Phys. *11*, 38–69.

Bott, A. (1989), *A positive definite advection scheme obtained by non-linear renormalization of the advective fluxes,* Monthly Weather Rev. *117*, 1006–1015.

Botta, N., Klein, R., Langenberg, S., and Lutzenkirchen, S. (2004), *Well balanced finite volume methods for nearly hydrostatic flows,* J. Comput. Phys. *196*, 539–565.

Boybeyi, Z., Ahmad, N., Bacon, D., Dunn, T., Hall, M., Lee, P., Sarma, A., and Wait, T. (2001), *Evaluation of the Operational Multiscale Environment Model with Grid Adaptivity against the European Tracer Experiment,* J. Appl. Meteorology *40,* 1541–1558.

Brooks, H. E. and Doswell, III, C. A. (1993), *Extreme winds in high-precipitation supercells,* Preprints of the *17th Conf. On Severe Local Storms,* Saint Louis, Missouri, pp. 173–177.

Carpenter, R. L., Droegemeier, K. K., Woodward, P. R., and Hane, C. E. (1990), *Application of the Piecewise Parabolic Method (PPM) to meteorological modeling,* Monthly Weather Rev. *118*, 586–612.

Collela, P. and Woodward, P. R. (1984), *The Piecewise Parabolic Method (PPM) for gas-dynamical simulations,* J. Comput. Phys. *54*, 174–201.

Durran, D. R. (1991), *The third-order Adams-Bashforth method: An attractive alternative to leapfrog time differencing,* Monthly Weather Rev. *119*, 702–720.

Emanuel, K. A. (1988), *The maximum intensity of hurricanes,* J. Atmosph. Sci. *45*, 1143–1155.

Gatski, T., Hussaini, M., and Lumley, J. (1996), *Simulation and Modeling of Turbulent Flows,* Oxford University Press.

Godunov, S. K. (1959), *A finite difference method for the computation of discontinuous solutions of the equations of fluid dynamics,* Matematicheskii Sbornik *47*, 357–393.

Gopalakrishnan, S. G., Bacon, D., Ahmad, N., Boybeyi, Z., Dunn, T., Hall, M., Lee, P., Madala, R., Sarma, A., Turner, M., and Wait, T. (2002), *An operational multiscale hurricane forecasting system.* Monthly Weather Rev. *130*, 1830–1847.

Harten, A., Lax, P., and van Leer, B. (1983), *On upstream differencing and Godunov-type schemes for hyperbolic conservation laws,* SIAM Rev. *25*, 35–61.

Harten, A. (1983), *High resolution schemes for hyperbolic conservation laws,* J. Comput. Phys. *49*, 357–393.

Holmes, D. G. and Connell, S. D. (1989), *Solution of the 2-D Navier-Stokes equations on unstructured adaptive grids,* AIAA Paper 89–1932.

Hubbard, M. E. and Nikiforakis, N. (2003), *A three-dimensional, adaptive, Godunov-type model for global atmospheric flows,* Monthly Weather Rev. *131*, 1848–1864.

Jameson, A., Schmidt, W., and Turkel, E. (1981), *Numerical solution of the Euler equations by finite volume method using Runge-Kutta time stepping schemes,* AIAA Paper 1981–1259.

Koračin, D., Isakov, V., and Mendez-Núñez, L. (1998), *A cloud-resolving model with the radiation scheme based on the Monte Carlo method,* Atmosph. Res. *47*, 437–459.

LeVeque, R. J., *Finite Volume Methods for Hyperbolic Problems* (Cambridge University Press (2002)). 558 pp.

Lilly, D. K. (1962), *On the numerical simulation of buoyant convection,* Tellus, *14*, 148–172.

LIN, S. J., CHAO, W. C., SUD, Y. C., and WALKER, G. K. (1994), *A class of van Leer-type transport schemes and its application to the moisture transport in a general circulation model,* Monthly Weather Rev. *122*, 1575–1593.

LUO, H., BAUM, J. D., and LÖHNER, R. (2003), *Extension of HLLC Scheme for Flows at all Speeds,* AIAA Paper 2003–3840.

MENDEZ-NÚÑEZ, L. R. and CARROLL, J. J. (1993), *Comparison of Leapfrog, Smolarkiewicz and MacCormacksSchemes applied to nonlinear equations,* Monthly Weather Rev. *121*, 565–578.

MENDEZ-NÚÑEZ, L. R. and CARROLL, J. J. (1994), *Application of the MacCormack scheme to atmospheric nonhydrostatic models,* Monthly Weather Rev. *122*, 984–1000.

MÜLLER, R. (1992), *The performance of classical versus modern finite volume advection schemes for atmospheric modeling in a one-dimensional test-bed*, Monthly Weather Rev. *120*, 1407–1415.

OOYAMA, K. V. (1990), *A thermodynamic foundation for modeling the moist atmosphere*. J. Atmosph. Sci. *47*, 2580–2593.

REISNER, J., WYSZOGRODZKI, A., MOUSSEAU, V., and KNOLL, D. (2003), *An efficient physics-based preconditioner for the fully implicit solution of small-scale thermally driven atmospheric flows,* J. Comput. Phys. *189*, 30–44.

SHAW, B. L., PIELKE, R. A., and ZIEGLER, C. L. (1997), *A three-dimensional numerical simulation of a great plains dryline,* Monthly Weather Rev. *125*, 1489–1506.

SMAGORINSKY, J. (1963), *General circulation experiments with the primitive equations,* Monthly Weather Rev. *91*, 99–164.

SMOLARKIEWICZ, P. K. (1984), *A fully multidimensional positive definite advection transport algorithm with small implicit diffusion,* J. Comput. Phys. *54*, 325–362.

SMOLARKIEWICZ, P. K. and SZMELTER, J. (2005), *MPDATA: An edge-based unstructured-grid formulation,* J. Comput. Phys. *206*, 624–649.

SOD, G. A. (1978), *A survey of several finite difference methods for systems of nonlinear hyperbolic conservation laws*, J. Comput. Phys. *27*, 1–31.

TAYLOR, T. D., NDEFO, E., and MASSON, B. S. (1972), *A study of numerical methods for solving viscous and inviscid flow problems,* J. Comput. Phys. *9*, 99–119.

TORO, E. F., SPRUCE, M., and SPEARES, W. (1994), *Restoration of the Contact Surface in the HLL Riemann Solver,* Shock Waves *4*, 25–34.

TORO, E. F., *Riemann Solvers and Numerical Methods for Fluid Dynamics,* (Springer-Verlag (1999)). 624 pp.

TREMBACK, C. J., POWELL, J., COTTON, W. R., and PIELKE, R. (1987), *The forward-in-time upstream advection scheme: Extension to higher orders,* Monthly Weather Rev. *115*, 540–555.

VAN LEER, B. (1999), *An Introduction to the Article "Reminiscences about Difference Schemes"* by S. K. Godunov, J. Comput. Phys. *153*, 1–5.

VAN LEER, B. (1979), *Towards the ultimate conservative difference scheme. V. A second-order sequel to Godunov's method*. J. Comput. Phys. *32*, 101–136.

ZALESAK, S. T. (1979), *Fully multidimensional flux-corrected transport algorithms for fluids,* J. Comput. Phys. *31*, 335–362.

(Received September 27, 2005, accepted June 5, 2006)